

# Performance of the Stereoscopic System of the HEGRA Imaging Air Čerenkov Telescopes: Monte Carlo Simulations & Observations

A. Konopelko<sup>a</sup>, M. Hemberger<sup>a</sup>, F. Aharonian<sup>a</sup>, A. Daum<sup>a</sup>,  
W. Hofmann<sup>a</sup>, C. Köhler<sup>a</sup>, H. Krawczynski<sup>a</sup>, H.J. Völk<sup>a</sup>,  
A. Akhperjanian<sup>b</sup>, J. Barrio<sup>c,d</sup>, K. Bernlöhr<sup>a</sup>, H. Bojahr<sup>f</sup>,  
J. Contreras<sup>d</sup>, J. Cortina<sup>d</sup>, T. Deckers<sup>e</sup>, S. Denninghoff<sup>c</sup>,  
J. Fernandez<sup>c,d</sup>, V. Fonseca<sup>d</sup>, J. Gonzalez<sup>d</sup>, V. Hausteijn<sup>g</sup>,  
G. Heinzelmann<sup>g</sup>, G. Hermann<sup>a</sup>, M. Heß<sup>a</sup>, A. Heusler<sup>a</sup>,  
H. Hohl<sup>f</sup>, I. Holl<sup>c</sup>, D. Horns<sup>g</sup>, R. Kankanian<sup>a,b</sup>, M. Kestel<sup>f</sup>,  
J. Kettler<sup>a</sup>, O. Kirstein<sup>e</sup>, H. Kornmayer<sup>c</sup>, D. Kranich<sup>c</sup>,  
H. Lampeitl<sup>a</sup>, A. Lindner<sup>g</sup>, E. Lorenz<sup>c</sup>, N. Magnussen<sup>f</sup>,  
H. Meyer<sup>f</sup>, R. Mirzoyan<sup>c,d</sup>, H. Möller<sup>f</sup>, A. Moralejo<sup>d</sup>,  
L. Padilla<sup>d</sup>, M. Panter<sup>a</sup>, D. Petry<sup>c,f</sup>, R. Plaga<sup>c</sup>,  
A. Plyasheshnikov<sup>a</sup>, J. Prahl<sup>g</sup>, C. Prosch<sup>c</sup>, G. Pühlhofer<sup>a</sup>,  
G. Rauterberg<sup>e</sup>, W. Rhode<sup>f</sup>, A. Röhring<sup>g</sup>, V. Sahakian<sup>b</sup>,  
M. Samorski<sup>e</sup>, J. Sanchez<sup>d</sup>, D. Schmele<sup>g</sup>, F. Schroeder<sup>f</sup>,  
W. Stamm<sup>e</sup>, B. Wiebel-Sooth<sup>f</sup>, C. A. Wiedner<sup>a</sup>, M. Willmer<sup>e</sup>,  
H. Wirth<sup>a</sup>, (HEGRA collaboration)

<sup>a</sup>*Max-Planck-Institut für Kernphysik, D-69029 Heidelberg, Germany*

<sup>b</sup>*Yerevan Physics Institute, 375036 Yerevan, Armenia*

<sup>c</sup>*Max-Planck-Institut für Physik, Föhringer Ring 6, D-80805 Munich, Germany*

<sup>d</sup>*Facultad de Ciencias Físicas, Universidad Complutense, E-28040 Madrid, Spain*

<sup>e</sup>*Universität Kiel, Inst. für Kernphysik, D-42118 Kiel, Germany*

<sup>f</sup>*BUGH Wuppertal, Fachbereich Physik, D-42119 Wuppertal, Germany*

<sup>g</sup>*Universität Hamburg, II. Inst. für Experimentalphysik, D-22761 Hamburg,  
Germany*

---

**Abstract**

Based on the Monte Carlo simulations we have studied the performance of the HEGRA system of imaging air Čerenkov telescopes (IACTs) in its present configuration of 4 IACTs as well as in its future final configuration of 5 IACTs. Here we present the results on the basic characteristics of the IACT system which are used in the standard data analysis procedure, i.e., the collection areas, the detection rates, the angular resolution, the energy resolution, and the  $\gamma$ /hadron-separation efficiency. By comparing several key Monte Carlo predictions with experimental results it is possible to check the accuracy of the simulations. The Monte Carlo results concerning hadron-nuclear showers are tested with the recorded cosmic ray events and the results concerning photon-induced showers are tested with a large data sample of  $\gamma$ -rays observed from BL Lac object Mkn 501 during its high flaring activity in 1997. Summarizing the simulations and current observations we give the basic recommendations of using the instrument and the major values of its sensitivity.

*PACS:* 95.55.Ka; 95.55.Vj; 96.40.Pq

*Keywords:* Imaging Air Čerenkov Technique; Very High Energy Gamma Ray Astronomy;

---

## 1 Introduction

The HEGRA collaboration is close to completing an array of five imaging air Čerenkov telescopes (IACTs) located on the Roque de los Muchachos, Canary Island La Palma (28.8° N, 17.9°). The telescope array, primarily designed for stereoscopic observations of the  $\gamma$ -radiation at energies above several hundred GeV [1] is formed by five identical IACTs - one at the center, and four others at the corners of a 100 m by 100 m square area. The multi-mirror reflector of each system telescope has an area of 8.5 m<sup>2</sup>. Thirty 60 cm diameter front aluminized and quartz coated spherical mirrors with focal length of about 5 m are independently installed on an almost spherical frame of an alt-azimuth mount. The FWHM of the point spread function of the reflector is better than 10 arcminutes. Each telescope is equipped with a 271-channel camera [2] with a pixel size of about 0.25° which results in the telescope's effective field of view of  $\simeq 4.3^\circ$ . The digitization of the PMT pulses is performed with a 120 MHz FADC system. The system trigger demands at least two neighboring pixels above the threshold in each of at least two telescopes. The present system of four telescopes is taking data in the stereoscopic mode since 1996 [3]. The whole telescope array of 5 IACTs is planned to run as a single detector at the end of 1998.

The basic concept of the HEGRA IACT array is the stereoscopic approach based on the simultaneous detection of air showers by  $\geq 2$  telescopes, which allows precise reconstruction of the shower parameters on an event-by-event basis, superior rejection of

hadronic showers, and effective suppression of the background light of different origins (night sky background, local muons, *etc.*). The recent observations of the Crab Nebula [3] and Mkn 501 [4] by the IACT system strongly support the theoretical expectations concerning the features of the stereoscopic imaging technique [5,6].

Due to the lack of a calibrated very high energy  $\gamma$ -ray beam, detailed Monte Carlo simulations are usually used for the design studies as well as for performance studies of the imaging atmospheric Čerenkov experiments. For example, new data analysis methods are developed and are tested with Monte Carlo simulations before being applied to real data. The measurement of absolute  $\gamma$ -ray flux and energy spectra of the established  $\gamma$ -ray sources as well as the determination of upper limits for the quiet objects heavily rely on Monte Carlo predictions of the detector performance. In the past, the comparison of the characteristics of recorded cosmic ray (CR) events with the characteristics of the Monte Carlo simulated hadron-induced air showers used to be the most reliable way to test the predictive power of the Monte Carlo simulations (e.g., [7]). Once the telescope response to CR-induced air showers is well understood, the Monte Carlo predictions for the  $\gamma$ -ray-induced shower can be performed with a high degree of confidence. The situation changed dramatically with the observation of the high flaring activity of Mkn 501 in 1997. The observations with the HEGRA system of 4 IACTs ( $\simeq 110$  h) provided a large data base of  $\gamma$ -rays ( $\geq 30000$ ) with unprecedented signal-to-noise ratio. Several observational key characteristics of  $\gamma$ -ray-induced air showers can be measured with small statistical uncertainties. The agreement of these key characteristics of  $\gamma$ -ray induced air showers in data and Monte Carlo simulations substantially strengthened the reliability of the simulations.

In this paper we discuss the standard data analysis procedure and the results of the detailed Monte Carlo simulations for the currently operating system of 4 IACTs as well as for the complete HEGRA array of 5 IACTs. Special attention has been paid on the proper simulation of the camera and electronics of the Čerenkov telescopes (see Section 2). Detailed comparisons of the detected cosmic ray and  $\gamma$ -ray-induced air showers with simulations have been made to understand the performance of the detector (Section 3). The basic characteristics of the HEGRA IACT system were calculated (Section 4). Finally, we discuss the resulting sensitivity of the HEGRA IACT array with respect to TeV  $\gamma$ -rays (Section 5) and summarize the basic recommendations for the use of the instrument.

## 2 Simulations

In the present calculations the complete Monte Carlo simulation procedure was divided into two steps. In the first step an extended library of simulated air showers, induced by different primaries, is produced. In the second step simulation of the response of the telescope camera pixels is applied to all generated events. The most time consuming step is evidently the first one, whereas the second step is relatively fast. This division allows to apply the detector simulation procedure several times to the generated showers in order to tune the Monte Carlo simulations to the hardware status of the telescopes (e.g. trigger

threshold, mirror adjustment etc.) Here we discuss the major features of this two-step simulation procedure.

### 2.1 Shower Simulation

The generation of the air showers has mainly been performed using the ALTAI Monte Carlo code [7]. For the electromagnetic cascade this code has implemented an algorithm based on the analytical probability distributions of the electron (positron) transport in the multiple-scattering segments. This algorithm substantially reduces the computational time needed for simulation of a single shower. The proton-nuclei cascade in the atmosphere is simulated according to the radial scaling model (RSM) based on accelerator data [8]. The air showers induced by the primary nuclei are simulated in a model of independent nucleon interactions for the fragmentation at the projectile-nucleus. The fragmentation of the colliding nuclei is processed according to the probabilities of different fragmentation channels. We studied the influence of the proton-nuclei cascade model on the observable shower parameters using the additional simulations with the CORSIKA code [9] which has implemented the HDPM model for the simulation of the nucleus-nucleus interactions.

The shower simulation is carried out at the level of single Čerenkov photons. A certain fraction ( $k \simeq 0.2$ ) of the Čerenkov photons of a shower which hit the telescope reflector are stored with full information, i.e. the arrival time, the arrival direction, and the impact coordinates in the reflector frame. By this means it is possible to apply the complete detector simulation procedure to all showers which have been processed in this way. The Monte Carlo library contains air showers induced by the primary  $\gamma$ -rays, protons, helium and other nuclei belonging to CNO, heavy and very heavy nuclei groups. The primary energy of the showers is randomly distributed inside 14 fixed energy bins covering the energy range from 100 GeV to 100 TeV. The events are used with weights according to some chosen primary spectra. The simulations have been performed for zenith angles  $0^\circ$ ,  $30^\circ$ ,  $45^\circ$ . For each type of primary particle and for each zenith angle approximately  $10^5$  showers were simulated. The actual setup of HEGRA IACT telescopes [3] was used in the simulations. The position of the shower axis in the observation plane was uniformly randomized over the area limited by the radius  $R_0$  with respect to the central telescope. The radius  $R_0$  was chosen between 250 and 450 m, increasing with shower energy and inclination angle. For the CR air showers the additional randomization over the solid angle around the telescope axis with the half opening angle of  $3.5^\circ$  has been introduced in order to reproduce the isotropic distribution of the CR events over the camera field of view.

### 2.2 Detector Simulation

The detector simulation procedure accounts for all efficiencies involved in the process of the Čerenkov light propagation which starts with emission of a Čerenkov photon and

ends with the digitization of the PMT signal (see for details [10]). The list of the effects which are important in this respect contains: (i) mirror reflectivity, modelled with the ray-tracing technique or in phenomenological way using the measured functions of the light spot distortion in the camera focal plane; (ii) the light absorption in the plexiglass panel covering the camera; (iii) the acceptance of the funnels placed in front of the photomultipliers (PMTs); (iv) the photon-to-photoelectron conversion inside the PMTs (EMI 9083R) taking into account a measured single photoelectron spectrum. The overall efficiency of the photon-to-photoelectron conversion is of  $\sim 0.1$ . By analogy with the experiment the structure of the readout based on the 120 MHz FADC data acquisition and the multiple-telescope trigger scheme [11] were implemented in the Monte Carlo simulations. Note, that this procedure takes into account the arrival times of the Čerenkov light photons hitting the telescope reflector. The basic characteristics of the performance of the telescope hardware, for instance the number of camera pixels read out for the triggered and none triggered telescopes, the single pixel rate and the single pixel trigger rate, the ratio between first and second maximum pixel amplitudes in the image etc have been directly compared between Monte Carlo and data [10].

### 3 Parameters of the Cosmic Ray Air Showers

The detection rate of the IACT system is mainly determined by the isotropic flux of primary cosmic ray protons and nuclei. The system is triggered if the shower produces a sufficiently high number of Čerenkov photons to trigger at least two telescopes. Since the number of Čerenkov photons produced by a shower is to first order approximation proportional to the energy of the primary particle, the trigger condition determines the energy threshold of the IACT system. At larger shower axis distances the Čerenkov photon density decreases rapidly. With increasing energy of the primary particles more and more showers are able to fulfill the trigger criteria, although they have impact distances far away from the telescope system. However, due to the steep primary energy spectrum of cosmic rays  $dJ_{cr}/dE \propto E^{-2.75}$  the contribution of the high energy showers ( $E > 20$  TeV) to the total cosmic ray detection rate is rather small even though they are collected over a larger area.

#### 3.1 Cosmic Ray Detection Rate

The basic characteristics of a single Čerenkov telescope at hardware level can be calculated using the procedure described in [12]. For a system of IACTs the only difference stems from the performance of the multi-telescope trigger. For this purpose, first the local trigger condition at each telescope as  $2n_n/271 > q_0$  (the signals in at least two neighboring pixels exceed  $q_0$ ) has to be fulfilled. The trigger threshold  $q_0$  is measured in photoelectrons. The system trigger demands for each individual event coincident trigger signals from at least  $N$  telescopes ( $N/5$ ,  $N = 2, 3, 4, 5$ ). Assuming the energy spectrum and the

chemical composition of the primary cosmic rays [13], the cosmic ray detection rate can be computed with the following formula:

$$R_{cr} = \int_0^{\Omega_0} d\Omega \, 2\pi \int_0^{R_0} R dR \int_0^{E_0} \frac{dJ_{cr}}{dE d\Omega dS} P_{cr}(R, E, \theta) \quad (1)$$

where  $E$  is the primary energy of a cosmic ray,  $R$  is the impact distance of the shower induced by the cosmic ray,  $\theta$  is the angle of the shower axis with respect to the telescope axis, and  $P_{cr}(R, E, \theta)$  is the probability of the shower to trigger the telescope system.

The performance of the multi-telescope trigger of the HEGRA IACT system was discussed in detail in [11]. In Table 1 we show the hardware detection rates for the different trigger thresholds as measured with the HEGRA telescope system [11] together with the results of the Monte Carlo simulations. The measured and computed rates are in a good agreement which confirms that the trigger procedure has been modelled correctly. Note that the absolute accuracy of the measured rate is about 0.2 Hz. The Monte Carlo predicted rates strongly rely on the used chemical composition and fluxes of the cosmic rays. So the accuracy of the Monte Carlo predicted rates is better than 20 %. The calculations of CR detection rates have been done also for the complete HEGRA system of 5 IACTs (see Table 2). One can see that the hardware detection rate for the complete array is expected to be approximately  $\simeq 1.4$  times larger than for the currently operating 4 IACT system.

### 3.2 Cosmic Ray Shower Images

The standard method to parametrize the Čerenkov light images was primarily introduced in [14]. It is based on the second moment analysis of the two-dimensional angular distributions of Čerenkov light flashes, sampled with pixels (PMTs) of finite solid angular extension [15]. The effective technique (supercuts) to extract the shower image from the measured matrix of the pixels amplitude was suggested in [16]. This method provides an effective  $\gamma$ /hadron separation and has been extensively used by several single Čerenkov telescopes around the world. For the system of IACTs the performance of the method can be substantially improved, as will be shown below.

The distributions of the second-moment image parameters depend crucially on the amount of background light per pixel. A slight overestimate or underestimate of the background light content dramatically change the distributions. The detailed detector simulation procedure is provided to account the exact background content in the camera pixels. In Figure 1 we show the distributions of the second-moment parameters of the cosmic ray images measured in the OFF region of Mrk 501 observations (dark sky region) by the HEGRA system of 4 IACT telescopes and the Monte Carlo simulations. It can be seen in Figure 1 that the Monte Carlo simulated images fit the measured images quite well.

In general, the distributions of the shape parameters of the Čerenkov light images depend

on the model of the development of the proton-nuclei cascade in the atmosphere and also on the model of the nucleus-nucleus interaction. To study this effect the series of simulations have been performed using the ALTAI code [7] and CORSIKA code (with HDPM model) [8] in the fragmentation model as well as under assumption of a simple superposition model of nucleus-nucleus interactions. The results show a good agreement of two simulation codes, despite of the very different models which are used for the simulations of the proton- nuclei component of the air showers. The distributions shown in Figure 1 have been produced assuming a certain chemical composition of the primary cosmic ray [13].

## 4 Imaging of the Gamma-Ray Air Showers

The hardware detection rate of the cosmic ray air showers dominates by at least two orders of magnitude over the detection rate of the  $\gamma$ -rays. To extract the  $\gamma$ -ray signal at sufficient confidence level, a special analysis is used to suppress significantly the rate of the cosmic ray events. This analysis is based on the application of several software cuts related to the orientation and the shape of the Čerenkov light images. Assuming an integral flux and an energy spectrum index of a  $\gamma$ -ray source, the detection rates of the  $\gamma$ -ray-induced air showers before and after application of the software cuts can be calculated.

### 4.1 Collection Areas and Detection Rates

One of the major advantages of the ground based Čerenkov technique in comparison with satellite observations is that the VHE  $\gamma$ -ray-induced air showers can be detected at large distances ( $\geq 100$  m) of the shower core from the telescope. That yields a high detection rate of the  $\gamma$ -ray-induced air showers which are distributed over the large area of  $S_\gamma \simeq 10^9$  cm<sup>2</sup> around the telescope site. The collection area for the  $\gamma$ -ray-induced air showers is calculated as

$$S_\gamma(E) = 2\pi \int_0^\infty P_\gamma(E, r) r dr \quad (2)$$

where  $P_\gamma(E, r)$  is the trigger efficiency of  $\gamma$ -ray-induced air showers of primary energy  $E$  and impact distance  $r$ . The collection area  $S_\gamma(E)$  for showers of primary energy  $E$ , is mainly determined by the effective area of the telescope reflector  $S_{ph.e.} = S_m \cdot \chi_{ph.e.}$ , where  $S_m$  is the total mirror area and  $\chi_{ph.e.}$  is the efficiency of the photon-to-photoelectron conversion of the camera channels. Given a fixed mirror area, a maximum collection area is achieved by reducing the trigger threshold of the telescopes. The latter is limited at the lower end by the fluctuations of the background light in each camera pixel.

In Figure 2 the collection areas for the complete HEGRA system of IACTs are shown for the conventional trigger criteria. The strong increase of collection area in the energy range  $\leq 1$  TeV changes to a logarithmic growth at higher energy. The behaviour of the collection areas is determined by the shape of the lateral distribution of the Čerenkov light pool at the observation level. The density of Čerenkov light photons at plateau for impact distances up to 125 m (for air showers observed at angles close to zenith) is roughly proportional to the primary shower energy whereas beyond 125 m the density of the Čerenkov light density decreases rapidly. In observations at large zenith angles ( $\geq 30$  degree) the collection area decreases at low energies ( $E \leq 3$  TeV) but increases at higher energies ( $E > 5$  TeV). The reason for that is that air showers at the larger zenith angles develop higher in the atmosphere. This is due to the fact that the same amount of the Čerenkov light (neglecting the increase in absorption) is produced by a shower, but is scattered over the larger area at the observation level which provides decreasing the density of Čerenkov photons. Thus low energy air showers at large zenith angles cannot trigger the telescopes but at the same time the high energy air showers have much larger collection area due to the large size of the Čerenkov light pool at observation level.

The HEGRA system of 5 imaging air Čerenkov telescopes has been designed for effective observation of  $\gamma$ -rays with the primary energy of several hundred GeV in stereoscopic mode with telescopes of relatively small mirror area, 8.5 m<sup>2</sup>. The system trigger based on the simultaneous detection of the shower images in several telescopes (at least 2) forces down the trigger threshold and consequently the energy threshold of the IACT system. Usually, the energy threshold is determined as the energy at which the detection rate of observed  $\gamma$ -ray showers reaches its maximum. For convenience we use in the following rate calculations a  $\gamma$ -ray spectrum according to:

$$dJ_\gamma/dE = A \cdot E^{-\alpha_\gamma}, \quad J_\gamma(> 1 \text{ TeV}) = 10^{-11} \text{ cm}^{-2}\text{s}^{-1}. \quad (3)$$

For a certain spectrum index  $\alpha_\gamma$  the  $\gamma$ -ray detection rate is calculated as

$$R_\gamma = \int_0^\infty \left(\frac{dR_\gamma}{dE}\right) dE = \int_0^\infty \left(\frac{dJ_\gamma}{dE}\right) S_\gamma(E) dE \quad (4)$$

where  $(dR_\gamma/dE)$  [Hz TeV<sup>-1</sup>] is the differential  $\gamma$ -ray detection rate.

Under the assumption of a differential index,  $\alpha_\gamma$ , of the  $\gamma$ -ray energy spectrum one can calculate the differential  $\gamma$ -ray detection rate  $(dR_\gamma/dE)$  (see Figure 3). The peak of the differential detection rate slightly shifts to higher energies with increase of the trigger multiplicity because low energy events cannot effectively trigger several telescopes. The integral detection rates of the  $\gamma$ -ray-induced air showers for different trigger multiplicities are presented in Table 3. Note that in the case of a steep  $\gamma$ -ray spectrum (e.g.  $\alpha_\gamma = 3.0$ ) for the system trigger 2/5 the  $\gamma$ -ray detection rate is much higher as compared with the operation for the 3/5 trigger mode. It is seen from Figure 3 that for the trigger conditions 2/5,  $2\text{nn}/271 > q_0$  ph.e. the differential detection rate peaks at an energy of  $\simeq 500$  GeV



which is identified as the energy threshold of the instrument. The energy threshold for observations at large zenith angles significantly increases (see Figure 4). At the same time, the rate of high energy events detected at large zenith angles could even exceed the corresponding rate in observations at the nominal zenith angles due to the significant increase of the collection area with increasing zenith angle.

Our Monte Carlo studies show that  $\gamma$ -ray air showers detected at large impact distance from the telescopes cause some difficulties for a reliable selection of  $\gamma$ -ray events. For plane-parallel  $\gamma$ -ray flux the Čerenkov light image shifts to the camera edge for large impact distances. These images are partially cut by the camera edge and cannot be used for an accurate reconstruction of the shower parameters (orientation of the shower axis in space, shower core location etc.). Thus for better evaluation of the energy spectrum it is useful to set a restriction on the reconstructed impact radius from the center of the system. This restriction influences mainly the collection areas at high energies. Above a certain energy the effective collection area is then determined simply by the geometrical area around the IACT system. The restriction on the impact distance for  $r < 200$  m in the case of steep spectrum does not significantly change the detection rate. For the case of a flat energy spectrum, especially at observations at large zenith angles, it is an advantage to collect  $\gamma$ -ray-induced air showers at large distances to the center of the IACT system.

#### 4.2 Reconstruction of Shower Arrival Direction

The simultaneous observations of the air showers with  $\geq 2$  imaging air Čerenkov telescopes offers the possibility to reconstruct the orientation of the shower axis with respect to the telescope axis [18]. The general approach is based on the superposition of the several images in one common focal plane in order to derive the intersection point of the major axis of the ellipsoid-like images. This intersection point determines the shower direction [6]. If the Čerenkov telescopes are directed towards the object, the reconstructed source position in the camera field of view for the  $\gamma$ -ray-induced air showers has to be in the center of the camera focal plane. The currently operating HEGRA system of IACTs performs so-called *wobble mode* observations. The position of the source in the camera focal plane is offset by  $0.5^\circ$  from the camera center (on declination) and consequently rotates depending on the azimuth angle. This approach gives the possibility to perform continuous ON source observations, whereas the OFF region can be chosen in  $1^\circ$  offset from the source position [3]. In present simulations the Čerenkov light images were shifted by  $0.5^\circ$  from the center of the focal plane with the correlated randomization over the azimuth.

The difference between the true and reconstructed position of the  $\gamma$ -ray source in the camera field of view,  $\Theta$ , is a measure of the angular resolution of the system of IACTs. The distributions of  $\Theta^2$ , both for the simulated and observed  $\gamma$ -ray showers from Mrk 501 are shown in Figure 5. One can see from Figure 5 both distributions match and both show a prominent peak around the source position. Our Monte Carlo studies show that the tail of the distribution at large  $\Theta^2$  is due to the air showers with the core positions close to the

line connecting two or three telescopes. In such a case, the images in the telescopes are almost parallel to each other and the reconstruction procedure leads to significant error in the evaluated shower direction because of a small intersection angle. Note that in the reconstruction procedure we require at least 3 telescopes have to be triggered (in addition we require also a minimum number of photoelectrons in the image of 40 ph.e.).

The angular resolution of the system of IACTs can be characterized quantitatively by the acceptance of the  $\gamma$ -ray-induced air showers,  $\kappa_{\gamma}^{dir}$ , after the application of the fixed angular cut on  $\Theta^2$ . In Table 4 the data on the acceptance,  $\kappa_{\gamma}^{dir}$ , of the  $\gamma$ -rays for three angular cuts  $\Theta^2 \leq 0.03, 0.05$  and  $0.1$  [deg<sup>2</sup>] are shown for the simulations at different zenith angles 0, 30, 45 degree. In general, for observations at large zenith angles the shower is far from the observer and the Čerenkov light images detected at large zenith angles have a smaller angular size, they are closer to the camera center and show almost circular shape. These changes in the image topology lead consequently to larger errors in the reconstruction of the shower direction. The comparison of the angular resolution for two different trigger multiplicities, 2/5 and 3/5, show some increase in the  $\gamma$ -ray acceptance applying the same angular cuts for the higher trigger multiplicity – 3/5. However, because of the energy dependence of the angular resolution two different system triggers have to be considered as complementary in observations of  $\gamma$ -ray sources with very different spectral features.

The angular resolution noticeably depends on the impact distance of the shower core from the center to the IACT system. For impact distances  $r \leq 125$  m the angular resolution slightly improves with increasing the energy of the  $\gamma$ -ray showers, because the images on average contain more light and the image orientation is better determined. The angular resolution,  $\delta\Theta$  (one standard deviation of the Gaussian distribution on  $\theta$ ), for  $\sim 1$  TeV  $\gamma$ -ray showers is of  $0.11^\circ$  and  $0.09^\circ$  at  $\sim 20$  and  $200$  m, respectively. Beyond  $\sim 120$  m the angular resolution decreases at higher energies. This can be explained by the distortion of the images by the edge of the limited camera field of view. The impact distances for high energy  $\gamma$ -rays correspond to large shifts of the images from the center of the camera focal plane (the high energy air showers occur deeper in the atmosphere). For  $\sim 10$  TeV  $\gamma$ -ray showers detected at impact distances of  $200$  m the angular resolution is  $0.14^\circ$ .

The advanced angular resolution of the HEGRA system of IACTs is a very effective tool for suppression of the isotropic cosmic ray background. The acceptances of cosmic ray air showers after application of an angular cut,  $\Theta^2 < \Theta_0^2$ , evaluated from the data taken with the currently operating HEGRA system of IACTs (OFF sample of Mrk 501) as well as from the Monte Carlo simulations are shown in Table 5. It is seen from Table 5 that after applying the angular cut of  $\Theta_0^2 = 0.03$  [deg<sup>2</sup>] the cosmic ray background rejection is as high as  $\simeq 200$ . One can see also from Table 5 that Monte Carlo simulations reproduce quite well the measured contamination of the cosmic ray air showers after application of an angular cut.

### 4.3 Localization of Shower Core

The position of the shower core at the observation level can be measured by the system of IACTs for a single individual event. Then the impact distances from the shower core to the system telescopes can be evaluated. The reconstruction algorithm is based on the orientation of the Čerenkov light images in several telescopes which have been triggered. We use pure geometric reconstruction which does not relate to the image shape. The accuracy of the shower core reconstruction is limited by the errors in the determination of the image orientation. As discussed before, the change of the Čerenkov light image topology leads to an increase of the error in the core position with increasing zenith angle. The accuracies of shower core reconstruction for the different primary energy and impact distance are summarized in Table 6. Observing a  $\gamma$ -ray source at zenith angles below 45 degrees and restricting the impact distances from the telescope to the shower core within 200 m the average accuracy is  $\leq 20$  m.

The reconstructed impact distance is used for calculating the image shape parameters scaled on an impact distance and image amplitude. These parameters are applied for the cosmic ray rejection. For that, the accuracy of 20 m is quite sufficient because the shape of the Čerenkov light images does not significantly change within 20 m. Furthermore, the value of the reconstructed impact distance is needed for evaluation of the shower energy. The calculations show that even with an accuracy of the shower core localization of around 20 m the energy resolution for  $\gamma$ -ray-induced air showers is better than 20%.

### 4.4 Measurement of Shower Energy

The procedure of energy reconstruction for the  $\gamma$ -ray-induced air showers observed with a single imaging air Čerenkov telescope appears to be quite complicated due to the lack of a direct measurements of the distance from the telescope to the shower core. Several indirect methods have been invented in order to estimate the impact distance using the centroid shift in the camera field of view as well as the image shape [19,20].

For the system of IACTs the measurement of the impact distance is straightforward and is not related to the image shape. That improves the accuracy in the energy reconstruction compared with a single telescope. The algorithms of the energy reconstruction for each individual event as well as for the spectrum evaluation with the system of IACTs have been discussed in [4,5,21]. This method of energy reconstruction was investigated by means of Monte Carlo simulations for the HEGRA system of IACTs.

If one can measure the distance from the shower core to the telescope ( $r_i, i = 1, N$ , where  $N$  is the number of triggered telescopes) the primary energy of air showers can be evaluated using the inverse function of the image size (amplitude) on shower energy and

impact distance

$$E_i = F(S_i, r_i, \theta) \quad (5)$$

where  $S_i$  is the image size (total number of photoelectrons in the image) and  $\theta$  is a zenith angle. The final energy estimate can be constructed by incorporating several images in a number of telescopes,  $E_i, i = 1, N$ , as  $E_0 = \sum_i w_i E_i$ , where  $w_i$  is an energy an core distance dependent weight ( $\sum w_i = 1$ ). Note that the energy resolution depends on the accuracy of determining the core distance and is strongly influenced by fluctuations in the image amplitude.

In Table 7 we show the estimates of the energy resolution in the different primary energy ranges as well as for the simulations at different zenith angles. Note that in a case of *wobble* mode observations the images of high energy  $\gamma$ -ray-induced air showers  $E \geq 10$  TeV are very often cut by the camera edge. This leads to a distortion in the impact distance reconstruction and consequently in the reconstruction of the shower energy. To remove this effect the large impact distances  $r \geq 200$  m are usually excluded from the consideration. For inclined showers (at large zenith angles) the Čerenkov light images are closer to the center of the field of view because these showers develop in atmosphere very far from the telescope and the corresponding images shrink to the camera center. Thus the problem of the camera edge appears to be less significant for inclined showers in the energy range at least up to 20 TeV. Data shown in Table 7 demonstrate that over the whole energy range for the  $\gamma$ -ray-induced air showers in observations at zenith angles up to 45 degrees the estimated energy resolution for the HEGRA system of IACTs is around 20%.

#### 4.5 Rejection of CR background using the image shape

Due to the difference in the nature of  $\gamma$ -ray- and proton/nuclei-induced air showers the corresponding Čerenkov light images are also very different in shape [22]. In the standard second-moment approach these differences can be determined by using such image shape parameters as *Width*, *Length* etc. The  $\gamma$ -ray-induced air showers have on average, images of smaller angular size. The selection of the  $\gamma$ -rays can be done by applying the standard *parameters cuts*:  $Width \leq w_0, Length \leq l_0$  etc where  $w_0, l_0$  are the boundaries which limit the domain of the most of the  $\gamma$ -ray-induced showers ( $\geq 50\%$ ).

When the minimum amplitude for the pixel used for the image parametrization is fixed, the parameters of the image shape would increase with the total number of photoelectrons in the image. For the high energy air showers more pixels are involved in the image parametrization procedure that is why the angular size of the image increases with the shower energy. Application of fixed *image shape cuts* saves the most of the low energy  $\gamma$ -rays (which are close to the energy threshold) and reduces significantly the content of high energy  $\gamma$ -rays. For the  $\gamma$ -ray spectrum evaluation that is undesirable because it will decrease the statistics of the observed high energy  $\gamma$ -rays. To avoid this problem the energy

dependent cuts have to be used. In addition, for a fixed primary energy of  $\gamma$ -ray-induced air showers the angular size of image also depends on the distance from the telescope to the shower core due to the decrease in image amplitude with impact distance. Thus for a single telescope using the restriction on the position of the image in a certain range from the camera center, one can keep only events at core distances  $r \leq 120$  m. The radial dependence of the angular size of an image is very small in this particular range of impact distances. However, such a restriction significantly reduces the number of detected  $\gamma$ -rays. For the system of IACTs both the energy and radial dependence of the image size can be accounted in detail, because the IACTs system measures the shower core position and consequently the energy for each individual event.

The images from the  $\gamma$ -ray-induced air showers can be sorted into several bins on the measured distance from the shower core,  $\Delta r_i, i = 1, n$ , and image size,  $\Delta \log(S_j), j = 1, m$ . Then the averaged image shape parameters are calculated for these particular bins,  $\langle w \rangle_{ij}, \langle l \rangle_{ij}$ . For an individual event the shower core position and impact distance from the shower core to the triggered telescopes can be reconstructed. Instead of the usual *Width* ( $w$ ) of the image the *scaled Width* [17] ( $\tilde{w}$ ) is calculated for each telescope and after that the *mean scaled Width* parameter is defined for this event:

$$\langle \tilde{w} \rangle = 1/N \sum_{k=1}^N w^k / \langle w \rangle_{ij}^k \quad (6)$$

where  $N$  is the number of triggered telescopes. The rejection of cosmic ray background events is performed by applying a cut on the *mean scaled Width*,  $\langle \tilde{w} \rangle \leq \langle \tilde{w}_0 \rangle$ . Measured distributions of the *mean scaled Width* for  $\gamma$ -ray-induced air showers observed at different zenith angles  $\leq 10, 30, 45$  degrees are shown in Figure 6. The distributions have a peak at 1.0 and are very narrow because after the *scaling* procedure the RMS of the distributions is determined only by the pure image fluctuations and does not depend any more on the image amplitude and shower impact distance. The multifold cut on the image *Width* is replaced by single parameter *mean scaled Width* and works effectively against the cosmic ray background events. For a single telescope (i.e. one view of the shower) the probability, that cosmic ray shower gives an image being very similar to the  $\gamma$ -ray-induced shower, could be as high as 0.1. In observations by several telescopes (in different projections) this probability is reduced down to  $10^{-2}$  (see Table 8). Note that in addition to *mean scaled Width cut* another shape parameters, such as *Length*, could be used. However, the simulations show that already after the *mean scaled Width cut* the cosmic ray background rejection is already very strong and an application of another shape cut does not improve the signal-to-noise ratio but simply reduces the amount of the  $\gamma$ -rays. The acceptances of the cosmic ray showers after the application of a mean scaled Width cut can be compared for Monte Carlo simulations and observed cosmic ray events. The data shown in Table 8 demonstrates a good agreement between the simulations and data.

There are two possible strategies for the choice of cuts. The first one is to apply the so-called strong cuts ( $\langle \tilde{w}_0 \rangle = 1.0$ ) which dramatically suppress the CR background but at

the same time also noticeably reduce the content of  $\gamma$ -rays (see Table 8). This approach works best when searching for the  $\gamma$ -ray signal from source candidates on a short time scale. For spectrum studies it is more effective to apply the loose cuts ( $\langle \tilde{w}_0 \rangle = 1.4$ ) which save most of the observed  $\gamma$ -rays at high energies and do not show strong energy dependent efficiencies (opposite to the tight cuts). It is important to note that the efficiency of the cosmic ray rejection improves approximately by a factor of 2 for 3-telescope events compared to 2-fold coincidence events while the decrease of the  $\gamma$ -ray acceptance is only of  $\simeq 20\%$ . Thus use of 3-fold events seems to be preferable from the point of view of the cosmic ray rejection using the image shape and orientation as well as for an accurate impact distance and energy reconstruction. However, in the specific case of the  $\gamma$ -ray fluxes characterized by very steep energy spectra the analysis of 2-fold coincidences could be applied in order to increase the statistics of  $\gamma$ -rays.

## 5 Sensitivity to $\gamma$ -ray fluxes

Using the calculated characteristics of the IACT system performance, one can estimate the sensitivity of the instrument in  $\gamma$ -ray observations. For two complementary approaches of the cosmic ray background rejection based on the application of *tight* and *loose* cuts the acceptances of the  $\gamma$ -rays and cosmic rays are shown in Table 9. For the integral flux of  $\gamma$ -rays taken at the level of  $J_\gamma(> 1 \text{ TeV}) = 10^{-11} \text{ cm}^{-2}\text{s}^{-1}$  the expected number of detected  $\gamma$ -rays per one hour is about 28 and 56 for the *tight* and *loose* cuts, respectively. For the *tight* cuts the cosmic rays are highly suppressed and the expected cosmic ray rate per hour is around 3 particles. Thus, the stereoscopic observations of  $\gamma$ -ray sources of an integral flux  $J_\gamma(> 1 \text{ TeV}) \geq 10^{-11} \text{ cm}^{-2}\text{s}^{-1}$  with the HEGRA array of IACTs are essentially *background free* (rate of the detected  $\gamma$ -rays exceeds the rate of the background event by more than a factor of 10). The expected sensitivity of the 5 IACT system for the  $\gamma$ -ray flux stated above after application of the *loose* cuts is about 5 “sigma-per-one-hour”. The  $5\sigma$  detection of  $\gamma$ -ray fluxes from point sources at the level of  $J_\gamma(> 1 \text{ TeV}) = 10^{-12} \text{ cm}^{-2}\text{s}^{-1}$  is possible in 20 hours of observations. Note, that after application of the *tight* cuts the amount of the detected cosmic electrons ( $\simeq 0.4$  particle per hour) becomes comparable to the cosmic ray contamination and further suppression of the background is limited by the electron content.

## 6 Summary

The HEGRA system of imaging air Čerenkov telescopes is the first instrument operating in the stereoscopic observation mode. The HEGRA system of 5 telescope with relatively small mirror area of  $8.5 \text{ m}^2$  gives a rather low energy threshold of  $\simeq 500 \text{ GeV}$ . The large camera field of view ( $\simeq 4.3$  degree) allows to perform the observations of the point  $\gamma$ -ray sources in the wobble mode, taking at the same time the ON and OFF events,

and increase the available observation time by a factor of two. The use of several images gives the angular resolution better than 0.1 degree and yields the cosmic ray rejection, using the shower orientation, up to 200 times. The geometrical reconstruction of the shower impact position with a good accuracy ( $\leq 20$  m) improves the energy resolution and makes possible to apply the image shape cuts which are independent on a shower energy. The energy reconstruction procedure for the telescope system is straightforward and is not related to the image shape. The energy resolution of the HEGRA system in the dynamic energy range of 0.5 GeV - 30 TeV is better than 20 %. In order to avoid the uncertainties in the evaluation of the energy spectrum of the detected  $\gamma$ -rays the effective collection area can be taken simply as the geometrical area around the center of the telescope system using the restriction on the reconstructed impact parameter (e.g., 200 m). Simultaneous registration of a several Čerenkov light images from the individual air shower makes possible to apply the correlated analysis of the image shape (mean scaled Width) and substantially improve the cosmic ray rejection up to 100. Note that the data analysis based on three coincidence view appears to be preferable for the better angular, energy resolution as well as gives better cosmic ray rejection using the image shape. The three coincidence events are optimum for the stereo imaging of the TeV  $\gamma$ -ray air showers. In the search mode the tight software cuts on shape and orientation show the better performance approaching the case of a background free detection of the  $\gamma$ -ray sources. However for the energy spectrum studies one can use the loose cuts providing the high  $\gamma$ -ray statistics.

The HEGRA system of IACTs could be considered as a successful prototype for the future low energy (100 GeV) arrays such as HESS and VERITAS. In general the current experience of the HEGRA operation can be used for the design of the forthcoming arrays of IACTs.

## 7 Acknowledgements

The support of the German Ministry for Research and Technology BMBF and of the Spanish Research Council CYCIT is gratefully acknowledged. We thank the Instituto de Astrofísica de Canarias for the use of the site and providing excellent working conditions. We gratefully acknowledge the technical support staff of Heidelberg, Kiel, Munich, and Yerevan.

We thank the anonymous referee for suggesting the improvements in the manuscript.

## References

- [1] Aharonian, F.A., 1993, in Proc. *Towards a Major Atmospheric Čerenkov Detector-II*, Calgary (ed. R.C.Lamb), 81.
- [2] Hermann, G., 1995, in Proc. *Towards a Major Atmospheric Čerenkov Detector-IV*, Padova (ed. M.Cresti), p. 396.
- [3] Daum, A., et al, 1998, *Astroparticle Physics*, Vol. 8, Nos. 1-2, p. 1
- [4] Aharonian, F.A., et al, 1997, *Astronomy & Astrophysics*, 327, L5-l8.
- [5] Aharonian, F.A., et al, 1994, *Experimental Astronomy*, 6, I: p. 343; II: p.369
- [6] Aharonian, F.A., Hofmann, W., Konopelko, A.K., Völk, H.J., 1997, *Astroparticle Physics*, 6, I: p. 343; II: p.369
- [7] Konopelko, et al., 1996, *Astroparticle Physics*, 4, 199.
- [8] Hillas, A.M., 1979, *Proc. 16 ICRC*, (Kyoto), 6, 13.
- [9] Capdevielle, J. et al, 1992, *Preprint KfK*, (Karlsruhe), 4998 p. 54
- [10] Hemberger, M., 1998, PhD thesis, Heidelberg.
- [11] Bulian, N., et al, 1998, *Astroparticle Physics*, (8)4, 223.
- [12] Aharonian, F.A., Hofmann, W., Konopelko, A.K., Plyasheshnikov, A.V., Ulrich, M., 1995, *J. Phys. G: Nucl. Part. Phys.* **21**, p. 419.
- [13] Wiebel, B. 1994, *Preprint WUB-94-08* (Wuppertal) 47 p.
- [14] Hillas, A.M., 1985, *Proc. 19th ICRC* (La Jolla) 1 p. 155
- [15] Reynolds, P.T., et al., 1993, *Astrophysical Journal*, 404, 206-218.
- [16] Punch, M., et al., 1992, *Nature*, Vol 358, 477.
- [17] Konopelko, A.K., 1995, in Proc. *Towards a Major Atmospheric Čerenkov Detector-IV*, Padova (ed. by M. Cresti), p. 373.
- [18] Hillas, A.M., 1989, in Proc. *Int. Workshop on VHE  $\gamma$ -ray astronomy*, Crimea, USSR, April 17-21, 1989, (eds. by A. Stepanian, D.J. Fegan, M.J. Cawley), p. 134.
- [19] Ulrich, M. 1995, in Proc. *Towards a Major Atmospheric Čerenkov Detector-V*, Padova (ed. by M. Cresti), p. 121.
- [20] le Bohec, S., 1995, in Proc. *Towards a Major Atmospheric Čerenkov Detector-IV*, Padova (ed. by M. Cresti), p. 378.
- [21] Hofmann, W., 1997, in Proc. *Towards a Major Atmospheric Čerenkov Detector-V*, Kruger National Park, South Africa (ed. by Okkie de Jager), p. 284.
- [22] Fegan, D.J., 1997, *J. Phys. G: Nucl. Part. Phys.*, **23**, 1013-1060



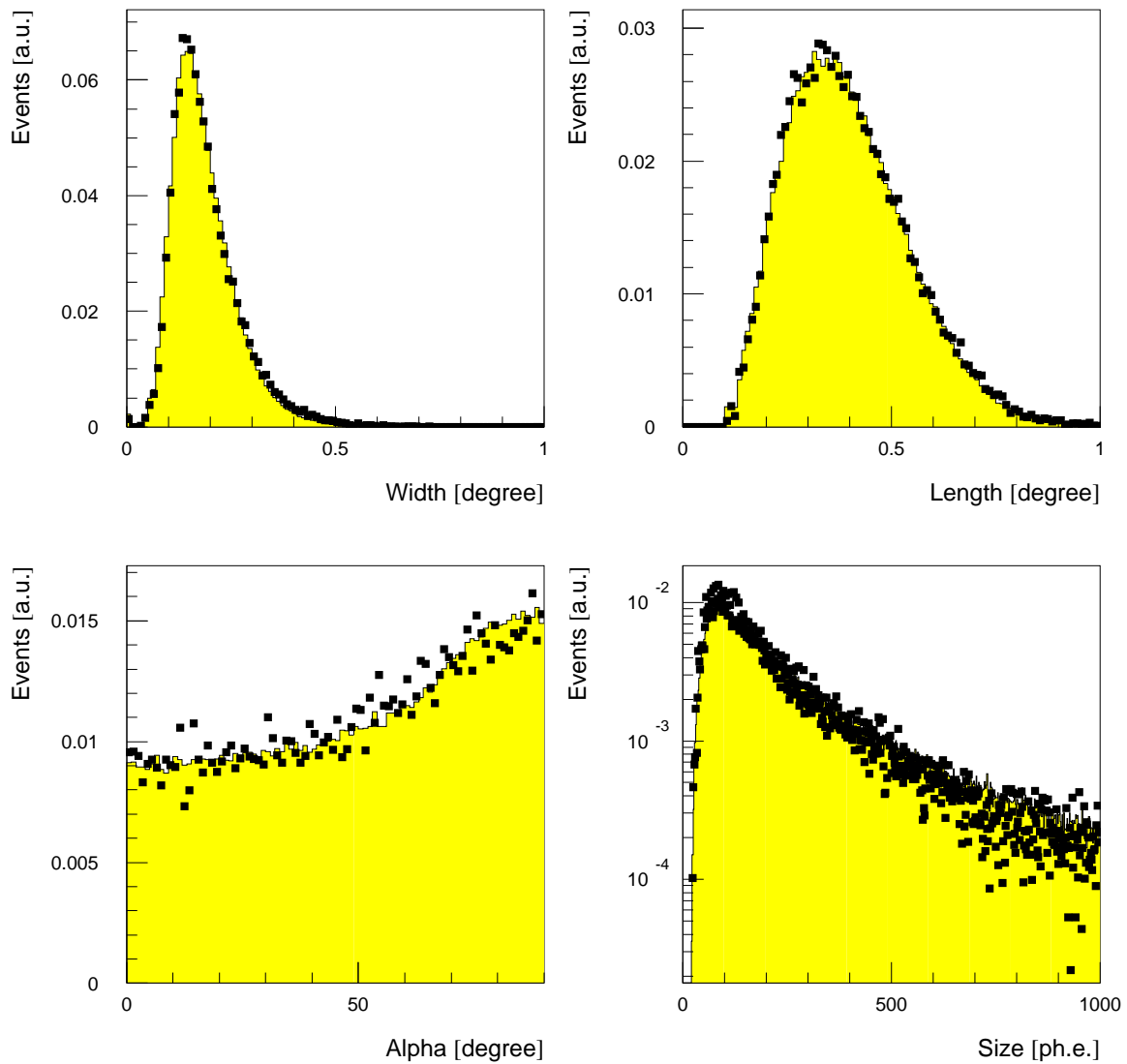


Fig. 1. Distributions of image parameters of the recorded cosmic ray air showers and of Monte Carlo simulated cosmic ray air showers at the zenith angles up to 30 degrees. The hatched histograms correspond to the data, the points are for the Monte Carlo simulations.

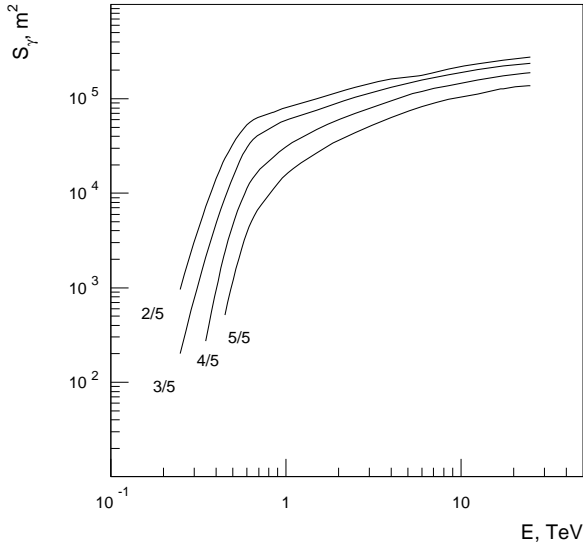


Fig. 2. Collection areas of the  $\gamma$ -ray-induced air showers simulated at zenith for the complete array of 5 HEGRA IACTs. Data correspond to different trigger multiplicities  $N = 2, 3, 4$  and  $5$  ( $N$  is a number of triggered telescope for an individual event). Local trigger for each telescope is taken as  $2nn/271 > 10$  ph.e.

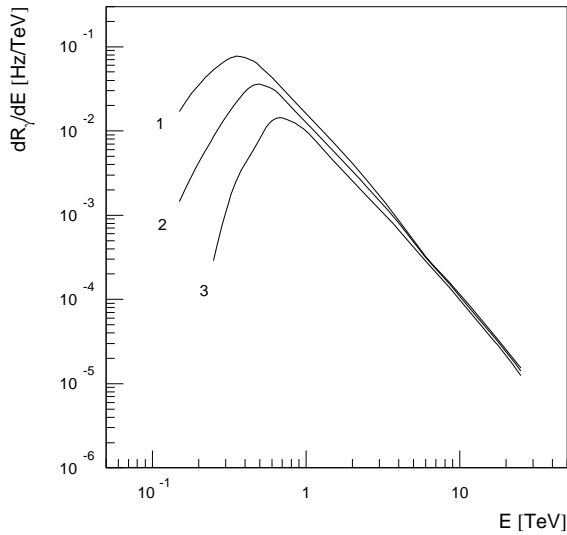


Fig. 3. The differential detection rates of  $\gamma$ -ray-induced air showers simulated at  $0^\circ$  zenith angle and detected by the system of 5 HEGRA IACTs operating with different local trigger condition:  $2/5$ ,  $2nn/271 > q_0$ ,  $q_0 = 8$  (1); 10 (2); 14 (3) ph. e. The assumed  $\gamma$ -ray spectrum is a power-law with the spectral index of 2.5 and with a flux normalization chosen according to Eqn. 4.

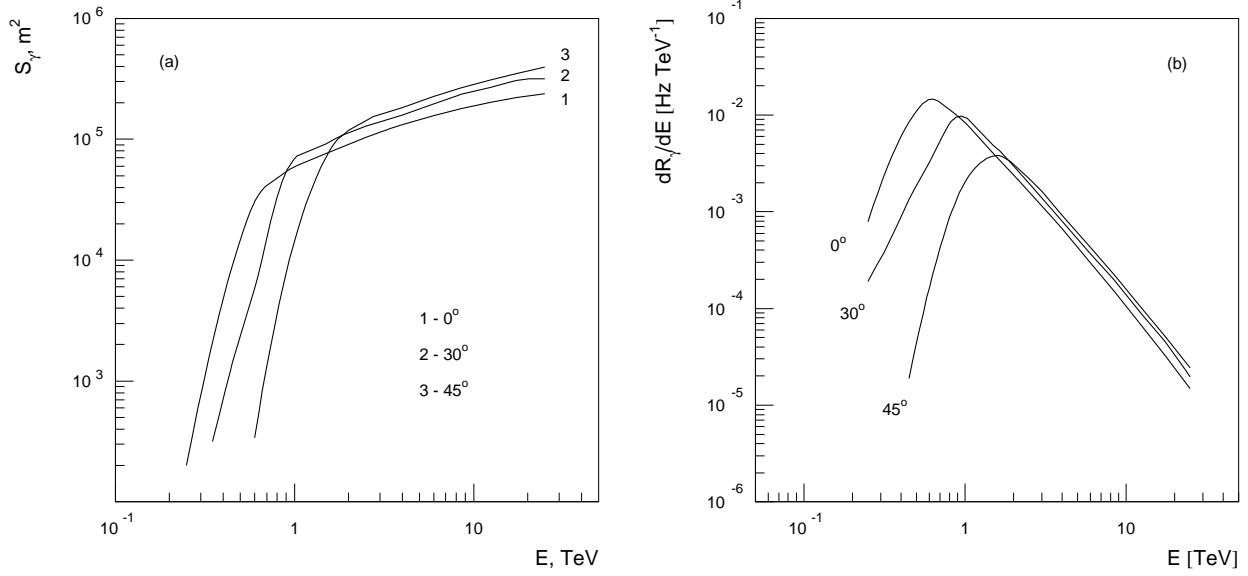


Fig. 4. The collection areas (a) and differential detection rates (b) for the  $\gamma$ -ray-induced air showers simulated at zenith angles  $0^\circ$ ,  $30^\circ$ ,  $45^\circ$  and system trigger:  $3/5$ ,  $2/271 > 10$  ph.e. The assumed  $\gamma$ -ray spectrum is a power-law with the spectral index of 2.5 and with a flux normalization chosen according to Eqn. 4.

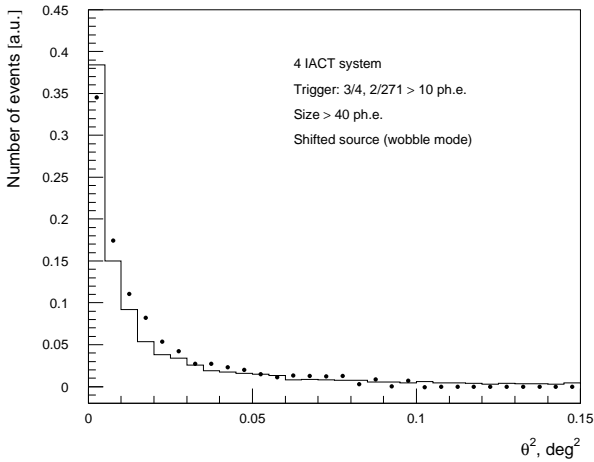


Fig. 5. Distribution of reconstructed arrival directions of the  $\gamma$ -ray-induced air showers.  $\Theta$  is an angular distance of the reconstructed position of the source in the camera focal plane from the true source position. The histogram corresponds to the Monte Carlo simulations. The distribution for  $\gamma$ -rays detected from Mrk 501 is indicated by black dots.

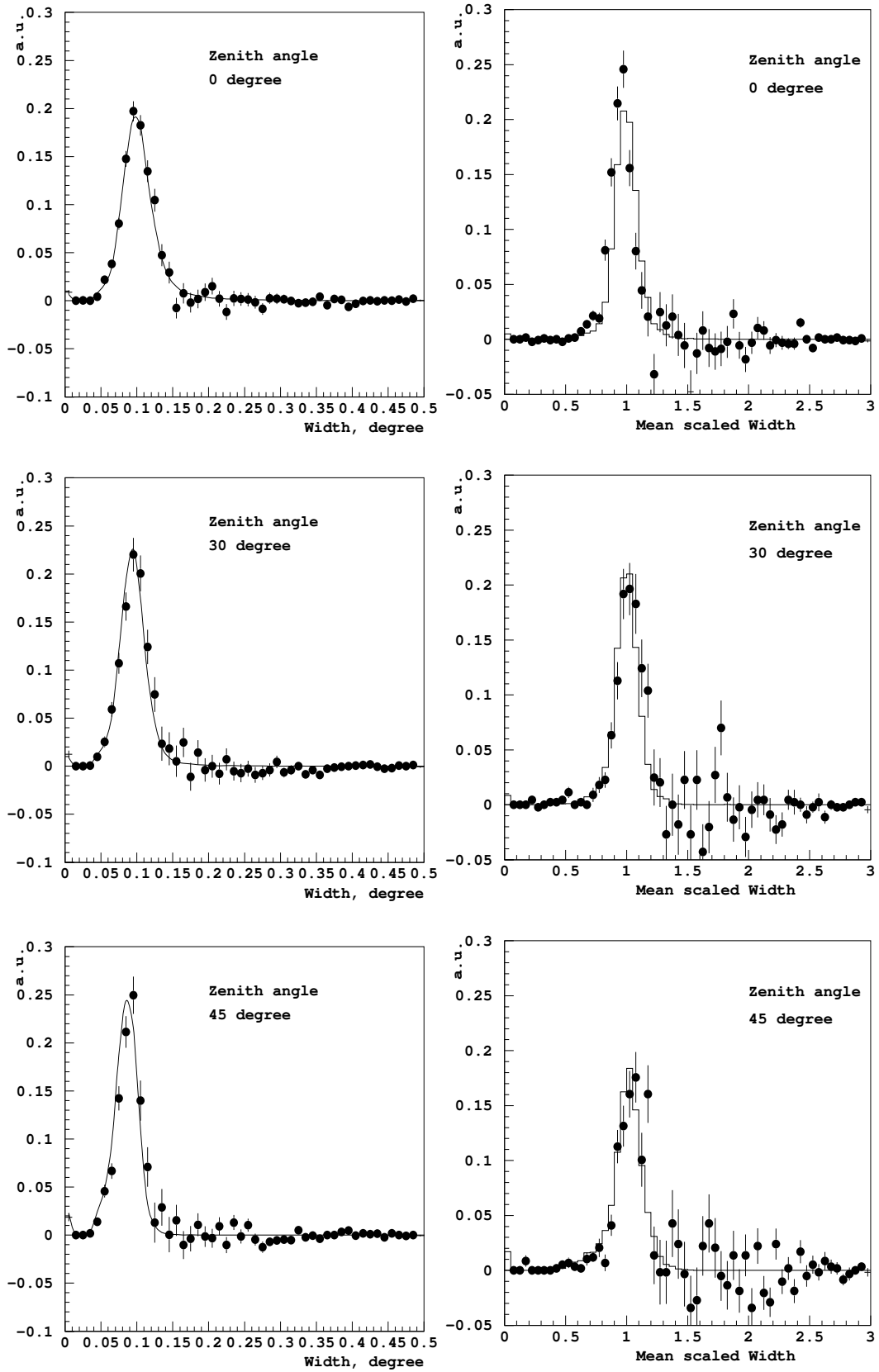


Fig. 6. Distributions of *Width* (left column) and *mean scaled Width* (right column) parameter of the  $\gamma$ -ray-induced air showers detected by the HEGRA IACT array (dots) at different zenith angles  $\sim 0, 30, 45$  degrees. Curves and histograms show the results of the Monte Carlo simulations.

Table 1

The cosmic ray detection rates,  $R_{\text{cr}}$  [Hz], for the currently operating HEGRA system of 4 IACTs in observations at the zenith angles up to 30 degree. The data correspond to the different multi-telescope triggers:  $N/4$  ( $N = 2, 3, 4$ ) in the case of trigger  $2nn/271 > q_0$  for each individual telescope. The measured rates are taken from [11] (data are interpolated for the particular trigger thresholds).

Trigger:	$q_0$ [ph.e.] =	8	10	15	30
2/4	(Data)	16.	9.6	5.5	2.4
	(MC)	18.	10.	5.6	2.0
3/4	(Data)	8.5	4.7	3.0	1.2
	(MC)	9.0	5.1	2.7	0.9
4/4	(Data)	3.8	1.8	1.3	0.5
	(MC)	3.6	1.9	1.0	0.3

Table 2

The cosmic ray detection rates,  $R_{\text{cr}}$  [Hz], for the complete system of 5 HEGRA IACTs calculated at the zenith angles up to 30 degree for different multi-telescope triggers,  $N/5$ , and for two trigger thresholds  $q_0 = 8, 10$  ph.e.

$q_0$ ph.e.	2/5	3/5	4/5	5/5
8	20.6	12.4	6.7	3.5
10	13.6	8.2	4.4	2.3

Table 3

The detection rates of the  $\gamma$ -ray-induced air showers,  $R_\gamma$  [photons/hour], for the complete HEGRA system of 5 IACTs for the different multi-telescope triggers. The local trigger for each individual telescope is set as  $2nn/271 > q_0$ ,  $q_0 = 10$  ph.e. The results correspond to a differential  $\gamma$ -ray spectrum in form of a power law with different spectrum index  $\alpha_\gamma$ .

$\alpha_\gamma$	2/5	3/5	4/5	5/5
2.0	75.6	54.0	32.4	19.4
2.5	97.2	61.2	34.2	17.3
3.0	133.2	79.2	36.0	17.6

Table 4

The Monte Carlo acceptance,  $\kappa_\gamma^{dir}$ , of the  $\gamma$ -ray-induced air showers simulated at different zenith angles,  $\theta$ , after application of the angular cut  $\Theta^2 < \Theta_0^2$  [deg<sup>2</sup>]. The calculations have been done for the system trigger of 2/5 and 3/5 and the local telescope trigger  $2nn/271 > 10$  ph.e. Additionally, the restriction on the distance of the shower core from the central telescope  $\leq 200$  m was applied.

Trigger:	$\Theta_0^2$	$\theta = 0^\circ$	$30^\circ$	$45^\circ$
	0.03	0.72	0.68	0.58
2/5	0.05	0.80	0.75	0.67
	0.10	0.89	0.87	0.81
	0.03	0.78	0.72	0.61
3/5	0.05	0.85	0.78	0.72
	0.10	0.92	0.89	0.84

Table 5

Acceptances of cosmic ray air showers,  $\kappa_{cr}^{dir}$ , after application of the angular cut,  $\Theta^2 < \Theta_0^2$ . Data and Monte Carlo (MC) simulations correspond to zenith angles up to 30 degree, system trigger 3/5 and the local telescope trigger  $2nn/271 > 10$  ph.e.

	$\Theta_0^2 = 0.01$	0.02	0.03	0.05	0.07	0.1
$\kappa_{cr}^{dir}$ (Data)	$1.7 \cdot 10^{-3}$	$3.4 \cdot 10^{-3}$	$5.1 \cdot 10^{-3}$	$8.6 \cdot 10^{-3}$	$1.2 \cdot 10^{-2}$	$1.7 \cdot 10^{-2}$
$\kappa_{cr}^{dir}$ (MC)	$2.1 \cdot 10^{-3}$	$4.1 \cdot 10^{-3}$	$5.5 \cdot 10^{-3}$	$9.0 \cdot 10^{-3}$	$1.2 \cdot 10^{-2}$	$1.8 \cdot 10^{-2}$

Table 6

Accuracy in localization of shower core of the  $\gamma$ -ray-induced air showers,  $\delta r$  (one standard deviation of the Gaussian approximation), simulated at different zenith angles,  $\theta$ , and impact distances from the center of IACT array,  $r$ . The impact distance ranges are numbered as 0-50 m (1); 50-100 m (2); 100-150 m (3); 150-200 m (4); 200-250 m (5).

$\theta$	E [TeV]	(1)	(2)	(3)	(4)	(5)
$\sim 30^\circ$	1-3	9	11	15	15	14
	3-5	5	6	11	17	15
	5-10	3	5	8	13	22
$45^\circ$	1-3	20	22	27	25	20
	3-5	11	14	22	30	26
	5-10	6	10	15	27	34

Table 7

Energy resolution,  $\Delta E/E$ , for  $\gamma$ -ray-induced air showers simulated at the zenith angles of 0, 30, 45 degrees. The maximum impact distance is 200 m. Data correspond to a system trigger of 3/5, and a local telescope trigger  $2nn/271 > 10$  ph.e.

$\theta$	$E_\gamma$ [TeV]	0.7-1	1-3	3-5	5-7	7-10	10-15	15-20
$30^\circ$		0.18	0.18	0.16	0.15	0.16	0.15	0.16
$45^\circ$			0.22	0.15	0.14	0.13	0.15	0.14

Table 8

The acceptance of the  $\gamma$ -rays,  $\kappa_\gamma$ , the cosmic ray background contamination,  $\kappa_{cr}$ , after application of a cut on *mean scaled Width*,  $\langle \tilde{w}_0 \rangle$ . The Monte Carlo simulations and data correspond to a zenith angle range up to 30 degree.

$\langle \tilde{w}_0 \rangle =$	0.95	1.0	1.1	1.2	1.3	1.4
$\kappa_\gamma$ (MC)	0.32	0.53	0.86	0.96	0.99	1.0
$\kappa_{cr}$ (Data)	0.008	0.011	0.027	0.074	0.145	0.26
$\kappa_{cr}$ (MC)	0.007	0.010	0.029	0.084	0.147	0.26

Table 9

The expected rates of  $\gamma$ -ray-induced and cosmic ray induced air showers, simulated at zenith angles up to 30 degree, before and after application of the angular and shape cuts. The estimated signal-to-noise ratio for the  $\gamma$ -ray source with the intensity of  $J_\gamma(> 1\text{TeV}) = 10^{-11}\text{cm}^{-2}\text{s}^{-1}$  (power-law spectrum index was taken as  $\alpha_\gamma = 2.5$ ). Data corresponds to the system trigger 3/5, the local telescope trigger  $2\text{nn}/271 > 10$  ph.e. and 200 m maximum distance from the shower axis.

*Tight cuts* ( $W_0 < 1.0$ ,  $\Theta_0^2 < 0.05$  [deg<sup>2</sup>]):

$i$	$R_i$ , Hz	$\kappa_i^{dir}$	$\kappa_i^{shape}$	$\tilde{R}_i$ , hour <sup>-1</sup>
$\gamma$	$1.7 \cdot 10^{-2}$	0.86	0.53	28
$CR$	7.8	0.009	0.01	3

*Loose cuts* ( $W_0 < 1.3$ ,  $\Theta_0^2 < 0.1$  [deg<sup>2</sup>]):

$i$	$R_i$ , Hz	$\kappa_i^{dir}$	$\kappa_i^{shape}$	$\tilde{R}_i$ , hour <sup>-1</sup>
$\gamma$	$1.7 \cdot 10^{-2}$	0.92	0.99	56
$CR$	7.8	0.018	0.15	76